DOI 10.1007/s12182-013-0284-3

Application of control volume based finite element method for solving the black-oil fluid equations

GHOREISHIAN AMIRI S A[1]*, SADRNEJAD S A[1], GHASEMZADEH H[1] and MONTAZERI G H[2]

[1] Faculty of Civil Engineering, K. N. Toosi University of Technology, Tehran, Iran
[2] Research and Development Dept., Iranian Central Oil Field Co., Tehran, Iran

Abstract: This is the second paper of a series where we introduce a control volume based finite element method (CVFEM) to simulate multiphase flow in porous media. This is a fully conservative method able to deal with unstructured grids which can be used for representing any complexity of reservoir geometry and its geological objects in an accurate and efficient manner. In order to deal with the inherent heterogeneity of the reservoirs, all operations related to discretization are performed at the element level in a manner similar to classical finite element method (FEM). Moreover, the proposed method can effectively reduce the so-called grid orientation effects. In the first paper of this series, we presented this method and its application for incompressible and immiscible two-phase flow simulation in homogeneous and heterogeneous porous media. In this paper, we evaluate the capability of the method in the solution of highly nonlinear and coupled partial differential equations by simulating hydrocarbon reservoirs using the black-oil model. Furthermore, the effect of grid orientation is investigated by simulating a benchmark waterflooding problem. The numerical results show that the formulation presented here is efficient and accurate for solving the bubble point and three-phase coning problems.

Key words: Control volume based finite element,black-oil model, grid orientation, porous media

1 Introduction

Prediction of performance for primary and secondary oil recovery processes has been one of the main concerns of reservoir engineers through the history of the petroleum industry. With the advent of high speed computing, reservoir simulators have proven to be invaluable tools to this end. In this respect, various flow models are employed by the reservoir simulators. These models range from simple single-phase flow models (Aronofsky and Jenkins, 1954) to sophisticated multiphase, multicomponent compositional flow models (Chen et al, 2006). Among these, the black-oil model is a standard three-phase flow model which is most often used by petroleum reservoir simulators. This is mainly because the black-oil model not only provides a reasonably general representation of the multicomponent, multiphase flow, but also avoids the necessity of using complicated phase equilibrium models.

The black-oil models consist of a set of partial differential equations describing the conservation of mass for the water, oil and gas components that generally coexist in a hydrocarbon reservoir, Darcy's law and equations of state. Since the equations are strongly nonlinear and coupled, their numerical solution is still a challenging task for reservoir engineers (Bergamaschi et al, 1998; Li et al, 2003; 2005; Naderan et al, 2007; Lee et al, 2008) even with the continual progress made in both computational algorithms and computer hardware.

A reliable numerical solution should be able to take into account the complexity of a real reservoir. The irregular geological and geometrical morphology of hydrocarbon reservoirs affect the computational domain. The reservoir permeability and porosity fields may experience very large local variation up to 8 or 10 orders of magnitude (Durlofsky et al, 1992) which results in highly discontinuous terms in the discretized form of the equations. This may lead the model to solve the equations inaccurately if the solution method is not appropriate. Moreover, the strongly nonlinear nature of the equations can produce highly diffusive non-physical oscillations at saturation fronts. The key solution for these issues is to develop a conservative numerical scheme which able to employ unstructured grids for spatial discretization.

Various numerical methods have been developed to model multiphase fluid flow through homogenous and heterogeneous porous media. The finite difference method (FDM) is the

*Corresponding author. email: sa_ghoreishian@dena.kntu.ac.ir
Received May 21, 2012

traditional framework for numerical simulation of multiphase flow in commercial simulators (Ewing, 1983; Coats et al, 1998; Cancelliere and Verga, 2012). The conventional FDM is influenced by the mesh quality and orientation which make it unattractive for unstructured gridding (Brand et al, 1991). Recently, multipoint approximation techniques have been developed to improve the accuracy of FDM on unstructured grids (Aavatsmark, 2002). However, application of these techniques for heterogeneous porous media is not demonstrated carefully.

Unstructured grids present an important step in reservoir simulation since there is no line or surface restriction in discretization of the physical domain. Unstructured meshes based on the finite volume method (FVM) (Edwards, 2002; Carvalho et al, 2007) or Galerkin-type FEM (e.g. Young, 1978) have been widely used in hydrocarbon reservoir simulations. The FVM is particularly attractive as it can conserve mass globally and locally. However, this method commonly requires additional treatments to model the flow in control volumes containing different permeable media (Monteagudo and Firoozabadi, 2007). On the other hand, treatment of the FEM in heterogeneous media is acceptable, but it does not conserve mass locally. Apart from the traditional FD, FV and FE methods, various combinations of these methods have been developed for reservoir simulation. Several multiphase flow and transport codes were developed based on the above mentioned numerical methods. Some of these codes and their specifications are summarized in Table 1.

Mass conservative schemes, such as the mixed finite element method (MFEM), CVFEM, control volume function approximation method (CVFAM), combination of finite element and finite volume method (FEFVM) and flux continuous finite volume method (FCFVM) have been extensively studied (Hoteit and Firoozabadi, 2008; Forsyth, 1990; Fung et al, 1992; Gottardi and Dall´Olio, 1992; Verma, 1996; Li et al, 2004; Geiger et al, 2004; Edwards and Rogers, 1998).

In the MFEM, pressures and velocities are approximated simultaneously with the same order of accuracy, while the saturation equation is generally solved using some shock capturing schemes. It is worth noting, application of this method for heterogeneous porous medium requires some additional treatments (Hoteit and Firoozabadi, 2008).

In the CVFAM, pressures and velocities are approximated independently with different interpolating functions and the saturation equation is solved using an upwind-type method. A higher order interpolating function is recommended to be applied in this method (Li et al, 2004) which results in an increase in computational cost.

In the FEFVM, the pressure and velocity problem is solved using MFEM or Galerkin FEM with some velocity recovery schemes, while the saturation equation is solved by a conservative FV scheme. In fact, a mesh system for FEM is constructed and a dual sub-grid system is then defined for

Table 1 Specifications of some frequently used multiphase flow and transport codes

Simulator	Developed in (Inst./ Comp.)	Spatial numerical solution method	Temporal numerical scheme	Type of gridding	Ref.
TOUGH2	Berkeley Lab Software Center	Integrated FDM	Fully implicit	Structured/ unstructured	Pruess et al (2012)
DuMu^{x}	University of Stuttgart	CVFEM	Fully implicit	Unstructured	Flemisch et al (2011)
OpenGeoSys (OGS)	UFZ/ BGR Hannover/ GFZ/ PSI/ Dresden University of Technology/ University of Tübingen/ Christian-Albrechts-University of Kiel/ University of Edinburgh/ KIGAM/ USGS	FEM	Implicit	Unstructured	Wang et al (2011)
CSMP^{++}	Imperial College/ Heriot-Watt University/ Montan University/ ETH Zurich	Hybrid FEM and FVM	IMPES*	Unstructured	Matthäi et al (2007)
GPRS	Reservoir Simulation Industrial Affiliate Program at Stanford University	CVFEM	Adaptive implicit	Structured/ unstructured	Durlofsky and Aziz (2004)
IPARS	Texas Institute for Computational and Applied Mathematics, The University of Texas at Austin	FD	Implicit	Structured	Lu et al (2001)
STOMP	Pacific Northwest National Laboratory	Integrated FDM	Fully implicit	Structured	White and Oostrom (2000)
SWMS-3D	U.S. Salinity Laboratory	FEM	Implicit explicit	Unstructured	Simbnek et al (1995)
MOFAT	Virginia Polytechnic Institute and State University	FEM	Implicit explicit	Unstructured	Katyal et al (1991)
BOAST	Keplinger and Associates, Inc./ The BDM Corporation	FD	IMPES	Structured	Fanchi et al (1982)

Notes: *IMPES: Implicit in pressure explicit in saturation

the FVM to take the advantage of the fact that fluid velocities which are discontinuous between two elements of the mesh, are continuous through the control volume faces of the FV grid (Durlofsky, 1993).

The numerical method used by Forsyth (1990), Fung et al (1992), Gottardi and Dall´Olio (1992) and Verma (1996) in petroleum reservoir simulation literature is called CVFEM. In most CVFEM employed in the field of reservoir simulation, the discrete equations of the multiphase flow system are obtained by integrating the equations of single-phase flow models, and then extending them by introducing the mobility terms. By considering this strategy, the method encounters some grid orientation problems which restricts the mesh angles to be equal or less than a right angle (Cordazzo et al, 2004a; 2004b). This restriction on mesh generation of the physical domain can be difficult to follow for most of the reservoirs due to their complex geometries. In addition, in common control volume finite element approaches the porous medium properties such as the absolute permeability and the porosity are stored in the center of the control volumes (Verma, 1996). If this strategy is considered for heterogeneous porous media, inter-nodal permeability evaluation will be required since the integration point lies on the interface of different materials. The problems related to the inter-nodal permeability evaluation are investigated by Romeu and Noetinger (1995) and Cordazzo et al (2003). Efficient treatment of a numerical scheme when it faces with discontinues material properties is a very important issue in modeling heterogeneous reservoirs such as fractured formations (e.g. Nick and Matthäi, 2011; Eikemo et al, 2009; Reichenberger et al, 2006).

The formulation presented here is derived directly from the multiphase flow equations in order to reduce the so-called grid orientation effects. Unlike the usual formulation on triangular and tetrahedral elements, any attempt of adapting the discretized equations to the conventional forms of FVM is discarded. Consequently, the concept of transmissibility is completely abandoned in the formulation.

In the first paper of this series (Sadrnejad et al, 2012), we developed a control volume based finite element method to solve the governing equations of incompressible two-phase fluid flow in heterogeneous porous media. The capability of the method to handle discontinuous material properties and its efficiency for capturing saturation fronts with minimum numerical dispersion and diffusion errors are evaluated by several numerical examples. In this paper, the proposed method is adopted for numerical solution of the black-oil fluid equations. This model is able to consider the compressibility and the mass transfer effects between the phases. The numerical results for the benchmark problems of the first and second SPE comparative solution projects (Odeh, 1981; Weinstein et al, 1986) are presented and compared with the reported solutions to evaluate the stability and convergence of the formulation. Moreover, the effects of grids orientation are investigated by a benchmark waterflooding problem.

2 Governing equations

In this section, the basic equations describing the black-oil model for reservoir simulation are derived based on the classical continuum theory of mixtures (Goodman and Gowin, 1972). The reservoir fluid is considered as a mixture of water, oil and gas phases. It is assumed that the only mass exchange occurs between oil and gas phases, and no mass transfer occurs between water and the other two phases. Furthermore, two distinct zones are considered in the porous medium, which are a dominant water-oil zone and a dominant oil-gas zone. The system in the water-oil zone is considered to be water-wet, while in the oil-gas zone is oil-wet.

The mass conservation equations are presented as

$$\frac{\partial\left(n_{\mathrm{w}}\rho_{\mathrm{w}}\right)}{\partial t}+\nabla.(n_{\mathrm{w}}\rho_{\mathrm{w}}\boldsymbol{w}_{\mathrm{w}})=\dot{M}_{\mathrm{w}} \tag{1}$$

for the water phase,

$$\frac{\partial\left(n_{\mathrm{o}}\rho_{\mathrm{o}}\right)}{\partial t}+\nabla.(n_{\mathrm{o}}\rho_{\mathrm{o}}\boldsymbol{w}_{\mathrm{o}})=\dot{m}_{\mathrm{og}}+\dot{M}_{\mathrm{o}} \tag{2}$$

for the oil phase, and

$$\frac{\partial\left(n_{\mathrm{g}}\rho_{\mathrm{g}}\right)}{\partial t}+\nabla.(n_{\mathrm{g}}\rho_{\mathrm{g}}\boldsymbol{w}_{\mathrm{g}})=-\dot{m}_{\mathrm{og}}+\dot{M}_{\mathrm{g}} \tag{3}$$

for the gas phase, where n_α, p_α, w_α, and $\dot{M}_\alpha$ represent the volume fraction, the mass density, the relative velocity and the source/sink terms of phase α [α: water (w) and oil (o) and gas (g)], respectively; and $\dot{m}_{\mathrm{og}}$ stands for the exchange of mass between the oil and gas phases. It is worth noting the source/sink terms ($\dot{M}_\alpha$) are calculated based on the well model presented by Wan (2002).

The water phase density is determined by

$$\rho_{\mathrm{w}}=\frac{\rho_{\mathrm{ws}}}{B_{\mathrm{wi}}}(1+C_{\mathrm{w}}(p_{\mathrm{w}}-p_{\mathrm{i}})) \tag{4}$$

where ρ_{ws} is the density of water at standard conditions; p_{w} is the water phase pressure; B_{wi} is the water formation volume factor at the initial formation pressure of p_{i}; and C_{w} represents the water compressibility factor. The gas phase density is calculated by

$$\rho_{\mathrm{g}}=\frac{\rho_{\mathrm{gs}}}{B_{\mathrm{g}}}\quad;\quad B_{\mathrm{g}}=\frac{ZT}{p_{\mathrm{g}}}\frac{p_{\mathrm{s}}}{T_{\mathrm{s}}} \tag{5}$$

where ρ_{gs} is the density of gas at standard conditions with pressure p_{s} and temperature T_{s}; B_{s} is the gas formation volume factor; Z is the deviation factor; T is the reservoir temperature; and p_{g} is the gas phase pressure. The oil phase density should be determined with respect to the fact that it consists of oil and gas components

$$\rho_{\mathrm{o}}=\frac{R_{\mathrm{so}}\rho_{\mathrm{gs}}+\rho_{\mathrm{os}}}{B_{\mathrm{o}}} \tag{6}$$

where ρ_{os} represents the density of the oil phase at the standard conditions; R_{so} is the gas solubility in the oil phase; and B_{o} is the oil formation volume factor.

The mass exchange term ($\dot{m}_{\mathrm{og}}$) in the mass balance equations, could be calculated as

$$\dot{m}_{\mathrm{og}}=\frac{\partial R_{\mathrm{so}}}{\partial t}\rho_{\mathrm{gs}}\frac{n_{\mathrm{o}}}{B_{\mathrm{o}}}=\frac{\partial R_{\mathrm{so}}}{\partial p_{\mathrm{o}}}\rho_{\mathrm{gs}}\frac{n_{\mathrm{o}}}{B_{\mathrm{o}}}\frac{\partial p_{\mathrm{o}}}{\partial t} \tag{7}$$

The relative velocity of each phase (regarding the solid phase) could be calculated by Darcy's law

$$n_\alpha \boldsymbol{w}_\alpha = \frac{k_{r\alpha}\boldsymbol{K}}{\mu_\alpha}\left[\rho_\alpha \boldsymbol{g} - \nabla p_\alpha\right] \tag{8}$$

where $\boldsymbol{K}$ is the absolute permeability tensor; $k_{r\alpha}$ and μ_α are the relative permeability and the dynamic viscosity of phase α, respectively.

In addition, there is a constraint for the fluid volume fractions

$$n_w + n_o + n_g = n \tag{9}$$

where n represents the rock porosity, and it is assumed to have the following form for the slightly compressible systems

$$n = n_i(1 + C_R(p - p_i)) \tag{10}$$

where n_i state the porosity at the reference pressure (p_i); C_R represents the rock compressibility; and p is the volume averaged pore pressure which has been defined by Pao et al (2001)

$$p = S_w p_w + S_o p_o + S_g p_g \tag{11}$$

where S_α represents the saturation of phase α. Replacing the phase saturations by the phase volume fractions, Eq. (11) can be written as

$$p = \frac{1}{n}(n_w p_w + n_o p_o + n_g p_g) \tag{12}$$

In order to specify the interacting motion of each phase on the other phases, constitutive equations are required which can link the fluid phase pressures to their volume fractions. According to Hassanizadeh and Gray (1993), the most practical method for considering this interacting motion is to use empirical correlations relating the capillary pressure (p_c) to the phase volume fractions. The capillary pressure is defined as the pressure difference of two immiscible fluids across their interface. For the water-oil zone, capillary pressure is indicated by $p_{cow}(= p_o - p_w)$, and for the oil-gas zone, capillary pressure is indicated by $p_{cgo}(= p_g - p_o)$. Following this, we can write

$$n_w = \mathrm{F}(p_{cow}) \tag{13}$$

$$n_l = \mathrm{F}(p_{cgo}) \tag{14}$$

where n_l represents the total liquid phase (water and oil) volume fraction:

$$n_l = n_w + n_o \tag{15}$$

Partially differentiating Eqs. (10), (13) and (14), one obtains

$$\begin{aligned} \mathrm{d}n = {} & \frac{n_i C_R}{n - n_i C_R}(n_w \,\mathrm{d}p_w + n_o \,\mathrm{d}p_o + \\ & n_g \,\mathrm{d}p_g + p_w \,\mathrm{d}n_w + p_o \,\mathrm{d}n_o + p_g \,\mathrm{d}n_g) \end{aligned} \tag{16}$$

$$\mathrm{d}n_w = \frac{\partial n_w}{\partial p_{cow}}(\mathrm{d}p_o - \mathrm{d}p_w) \tag{17}$$

$$\mathrm{d}n_l = \frac{\partial n_l}{\partial p_{cgo}}(\mathrm{d}p_g - \mathrm{d}p_o) \tag{18}$$

and from Eqs. (15) and (9) we have

$$\mathrm{d}n_o = \mathrm{d}n_l - \mathrm{d}n_w \tag{19}$$

$$\mathrm{d}n_g = \mathrm{d}n - \mathrm{d}n_l \tag{20}$$

substituting Eq. (16) into Eq. (19), one obtains

$$\mathrm{d}n_o = \frac{\partial n_l}{\partial p_{cgo}}(\mathrm{d}p_g - \mathrm{d}p_o) - \frac{\partial n_w}{\partial p_{cow}}(\mathrm{d}p_o - \mathrm{d}p_w) \tag{21}$$

for the evolution of oil volume fraction. Substituting Eqs. (17) and (21) into Eq. (16), and then substituting the result into Eq. (20), one obtains the following relation for the evolution of gas volume fraction

$$\begin{aligned} \mathrm{d}n_g = {} & \frac{n_i C_R}{n - n_i C_R(1 + p_g)} \times \\ & \left[\left(n_o - n'_w p_{cow} + n'_l\left(\frac{n - n_i C_R}{n_i C_R} - p_o\right)\right)\mathrm{d}p_o \right. \\ & \left. + \left(n_w + n'_w p_{cow}\right)\mathrm{d}p_w + \left(n_g + n'_l\left(p_o - \frac{n - n_i C_R}{n_i C_R}\right)\right)\mathrm{d}p_g\right] \end{aligned} \tag{22}$$

The final form of the flow equations can be simply developed by substituting Eqs. (4)-(8), (17), (21) and (22) into Eqs. (1)-(3) as below

$$\begin{aligned} & \left(\frac{n_w \rho_{ws}}{B_{wi}} C_w - n'_w \rho_w\right)\frac{\partial p_w}{\partial t} + \left(n'_w \rho_w\right)\frac{\partial p_o}{\partial t} \\ & + \nabla.\left\{\rho_w \boldsymbol{K}_w\left(\rho_w \boldsymbol{g} - \nabla p_w\right)\right\} - \dot{M}_w = 0 \end{aligned} \tag{23}$$

for the water phase, in which

$$n'_w = \frac{\partial n_w}{\partial p_{cow}} \tag{24}$$

$$\boldsymbol{K}_w = \frac{k_{rw}\boldsymbol{K}}{\mu_w} \tag{25}$$

similarly, for the oil phase

$$\begin{aligned} & \left(n'_w \rho_o\right)\frac{\partial p_w}{\partial t} + \left[n_o\left(\frac{\rho_{gs} R'_{so}}{B_o} - B'_o \frac{R_{so}\rho_{gs} + \rho_{os}}{B_o^2}\right) - \right. \\ & \left. (n'_l + n'_w)\rho_o - n_o \frac{R'_{so}\rho_{gs}}{B_o}\right]\frac{\partial p_o}{\partial t} + \left(n'_l \rho_o\right)\frac{\partial p_g}{\partial t} + \\ & \nabla^{\mathrm{T}}\left[\rho_o \boldsymbol{K}_o\left(\rho_o \boldsymbol{g} - \nabla p_o\right)\right] - \dot{M}_o = 0 \end{aligned} \tag{26}$$

in which

$$n'_l = \frac{\partial n_l}{\partial p_{cgo}} \tag{27}$$

$$R'_{so}=\frac{\partial R_{so}}{\partial p_o} \tag{28}$$

$$B'_o=\frac{\partial B_o}{\partial p_o} \tag{29}$$

$$\boldsymbol{K}_o=\frac{k_{ro}\boldsymbol{K}}{\mu_o} \tag{30}$$

and finally, for the gas phase

$$\begin{aligned}&\left[\rho_g\frac{n_iC_R}{n-n_iC_R(1+p_g)}\left(n_w+n'_w p_{cow}\right)\right]\frac{\partial p_w}{\partial t}+\\&\left[\rho_g\frac{n_iC_R}{n-n_iC_R(1+p_g)}\left(n_o-n'_w p_{cow}+n'_l\left(\frac{n-n_iC_R}{n_iC_R}-p_o\right)\right)+\right.\\&\left.n_o\frac{R'_{so}\rho_{gs}}{B_o}\right]\frac{\partial p_o}{\partial t}+\left[\rho_g\frac{n_iC_R}{n-n_iC_R(1+p_g)}\times\right.\\&\left.\left(n_g+n'_l\left(p_o-\frac{n-n_iC_R}{n_iC_R}\right)\right)+n_g\frac{B'_g\rho_{gs}}{B_g^2}\right]\frac{\partial p_g}{\partial t}+\\&\nabla^T\left[\rho_g\boldsymbol{K}_g\left(\rho_g\boldsymbol{g}-\nabla p_g\right)\right]-\dot{M}_g=0\end{aligned} \tag{31}$$

in which

$$B'_g=\frac{\partial B_g}{\partial p_g} \tag{32}$$

$$\boldsymbol{K}_g=\frac{k_{rg}\boldsymbol{K}}{\mu_g} \tag{33}$$

Eqs. (23), (26) and (31) represent a system of highly nonlinear and coupled equations describing the black-oil flow in a hydrocarbon reservoir. The major sources of nonlinearities in these equations, i.e. the phase volume fraction (n_α), and relative permeability (k_α) are strongly dependent on the primary unknown variables and therefore should be continuously updated during the solution procedure. However, effects of the weak nonlinearities, i.e. the formation volume factor (B_α), viscosity (μ_α), gas solubility (R_{so}), and porosity (n) could not be neglected. Treatment of these two types of nonlinearities is carefully described by Settari and Aziz (1975). In order to complete the description of the governing equations, it is necessary to define appropriate initial and boundary conditions. The initial conditions specify the full field of phase pressures at time t=0

$$p_\alpha=p_\alpha^0 \quad \text{in } \Omega \text{ and on } \Gamma \tag{34}$$

where Ω is the domain of interest and Γ is its boundary. The boundary condition can be of two types or a combination of these: the Dirichlet boundary condition, in which the phase pressures on the boundaries (Γ_p) are known, and the Neumann boundary condition, in which the values of phase fluxes at the boundaries (Γ_q) are imposed (where $\Gamma=\Gamma_p\cup\Gamma_q$)

$$p_\alpha=\bar{p}_\alpha \quad \text{on } \Gamma_p \tag{35}$$

$$\left[\rho_\alpha\boldsymbol{K}_\alpha(\rho_\alpha\boldsymbol{g}-\nabla p_\alpha)\right]^T.\boldsymbol{n}=\bar{\boldsymbol{q}}_\alpha \quad \text{on } \Gamma_q \tag{36}$$

where $\boldsymbol{n}$ denotes the outward unit normal vector on the boundary and $\bar{\boldsymbol{q}}$ is the imposed mass flux which is normal to the boundary.

3 Numerical solution

Discretization of the governing equations can be now expressed by the use of the CVFEM developed by Sadrnejad et al (2012) in terms of the nodal phase pressures (i.e. $\hat{\boldsymbol{p}}_\alpha$) which are selected as the primary variables. In this method, the physical domain is discretized using hexahedral elements (Fig. 1(a)), and further subdivision of the elements into control volumes is performed in the transformed space (Fig. 1(b)). Furthermore, in order to represent the discretized equations at the element level (instead of the control volume level), the control volumes are also divided into sub-control volumes. Each of these sub-control volumes belongs to a specific element which is in association with the given control volume (Fig. 1(c)).

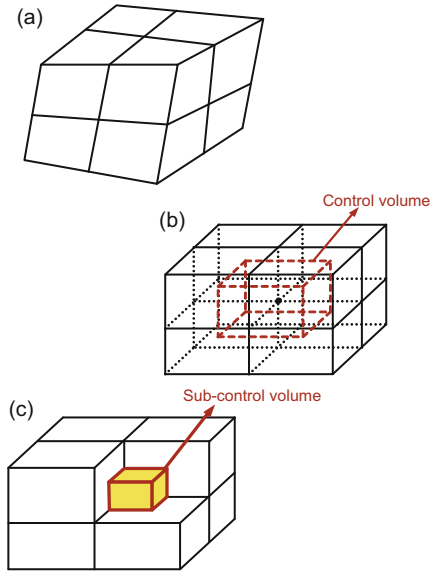

Fig. 1 (a) System of finite element mesh in the physical space; (b) representation of control volume around a node in the transformed space; (c) illustrating a sub-control volume belongs to the eliminated element (after Sadrnejad et al, 2012)

The values of phase pressures (p_α) at any point within an element are approximated by the following expression

$$p_\alpha(\xi,\eta,\zeta)=\boldsymbol{N}(\xi,\eta,\zeta)\hat{\boldsymbol{p}}_\alpha \tag{37}$$

where $\boldsymbol{N}(\xi,\eta,\zeta)$ is the vector of standard finite element shape functions.

CVFE discretization procedure, as presented by Sadrnejad et al (2012), when applied to Eqs. (23), (26) and (31) along with the boundary condition (36), they yield

$$\begin{bmatrix} \bar{\boldsymbol{P}}_{\mathrm{ww}} & 0 & 0 \\ 0 & \bar{\boldsymbol{P}}_{\mathrm{oo}} & 0 \\ 0 & 0 & \bar{\boldsymbol{P}}_{\mathrm{gg}} \end{bmatrix} \begin{bmatrix} \hat{\boldsymbol{p}}_{\mathrm{w}} \\ \hat{\boldsymbol{p}}_{\mathrm{o}} \\ \hat{\boldsymbol{p}}_{\mathrm{g}} \end{bmatrix} + \begin{bmatrix} \boldsymbol{P}_{\mathrm{ww}} & \boldsymbol{C}_{\mathrm{wo}} & 0 \\ \boldsymbol{C}_{\mathrm{ow}} & \boldsymbol{P}_{\mathrm{oo}} & \boldsymbol{C}_{\mathrm{og}} \\ \boldsymbol{C}_{\mathrm{gw}} & \boldsymbol{C}_{\mathrm{go}} & \boldsymbol{P}_{\mathrm{gg}} \end{bmatrix} \frac{\mathrm{d}}{\mathrm{d}t} \begin{bmatrix} \hat{\boldsymbol{p}}_{\mathrm{w}} \\ \hat{\boldsymbol{p}}_{\mathrm{o}} \\ \hat{\boldsymbol{p}}_{\mathrm{g}} \end{bmatrix} = \begin{bmatrix} \boldsymbol{f}_{\mathrm{w}} \\ \boldsymbol{f}_{\mathrm{o}} \\ \boldsymbol{f}_{\mathrm{g}} \end{bmatrix} \tag{38}$$

where the coefficients are described as

$$\bar{\boldsymbol{P}}_{\mathrm{ww}} = -\int_{\Gamma_{\mathrm{S.C.V.}}-\Gamma_{\mathrm{q}}} \boldsymbol{W}^{\mathrm{T}} \left\{ \left(\rho_{\mathrm{w}} \boldsymbol{K}_{\mathrm{w}} \nabla \boldsymbol{N} \right)^{\mathrm{T}} . \boldsymbol{n} \right\}^{\mathrm{T}} \mathrm{d}\Gamma \tag{39}$$

$$\bar{\boldsymbol{P}}_{\mathrm{oo}} = -\int_{\Gamma_{\mathrm{S.C.V.}}-\Gamma_{\mathrm{q}}} \boldsymbol{W}^{\mathrm{T}} \left\{ \left(\rho_{\mathrm{o}} \boldsymbol{K}_{\mathrm{o}} \nabla \boldsymbol{N} \right)^{\mathrm{T}} . \boldsymbol{n} \right\}^{\mathrm{T}} \mathrm{d}\Gamma \tag{40}$$

$$\bar{\boldsymbol{P}}_{\mathrm{gg}} = -\int_{\Gamma_{\mathrm{S.C.V.}}-\Gamma_{\mathrm{q}}} \boldsymbol{W}^{\mathrm{T}} \left\{ \left(\rho_{\mathrm{g}} \boldsymbol{K}_{\mathrm{g}} \nabla \boldsymbol{N} \right)^{\mathrm{T}} . \boldsymbol{n} \right\}^{\mathrm{T}} \mathrm{d}\Gamma \tag{41}$$

$$\boldsymbol{P}_{\mathrm{ww}} = \int_{\Omega_{\mathrm{e}}} \boldsymbol{W}^{\mathrm{T}} \left(\frac{n_{\mathrm{w}} \rho_{\mathrm{ws}}}{B_{\mathrm{wi}}} C_{\mathrm{w}} - n'_{\mathrm{w}} \rho_{\mathrm{w}} \right) \boldsymbol{N} \, \mathrm{d}\Omega \tag{42}$$

$$\boldsymbol{P}_{\mathrm{oo}} = \int_{\Omega_{\mathrm{e}}} \boldsymbol{W}^{\mathrm{T}} \left(n_{\mathrm{o}} \left(\frac{\rho_{\mathrm{gs}} R'_{\mathrm{so}}}{B_{\mathrm{o}}} - B'_{\mathrm{o}} \frac{R_{\mathrm{so}} \rho_{\mathrm{gs}} + \rho_{\mathrm{os}}}{B_{\mathrm{o}}^2} \right) - (n'_{\mathrm{l}} + n'_{\mathrm{w}}) \rho_{\mathrm{o}} - n_{\mathrm{o}} \frac{R'_{\mathrm{so}} \rho_{\mathrm{gs}}}{B_{\mathrm{o}}} \right) \boldsymbol{N} \, \mathrm{d}\Omega \tag{43}$$

$$\boldsymbol{P}_{\mathrm{gg}} = \int_{\Omega_{\mathrm{e}}} \boldsymbol{W}^{\mathrm{T}} \left[\rho_{\mathrm{g}} \frac{n_{\mathrm{i}} C_{\mathrm{R}}}{n - n_{\mathrm{i}} C_{\mathrm{R}} (1 + p_{\mathrm{g}})} \left(n_{\mathrm{g}} + n'_{\mathrm{l}} \left(p_{\mathrm{o}} - \frac{n - n_{\mathrm{i}} C_{\mathrm{R}}}{n_{\mathrm{i}} C_{\mathrm{R}}} \right) \right) + n_{\mathrm{g}} \frac{B'_{\mathrm{g}} \rho_{\mathrm{gs}}}{B_{\mathrm{g}}^2} \right] \boldsymbol{N} \, \mathrm{d}\Omega \tag{44}$$

$$\boldsymbol{C}_{\mathrm{wo}} = \int_{\Omega_{\mathrm{e}}} \boldsymbol{W}^{\mathrm{T}} \left(n'_{\mathrm{w}} \rho_{\mathrm{w}} \right) \boldsymbol{N} \, \mathrm{d}\Omega \tag{45}$$

$$\boldsymbol{C}_{\mathrm{ow}} = \int_{\Omega_{\mathrm{e}}} \boldsymbol{W}^{\mathrm{T}} \left(n'_{\mathrm{w}} \rho_{\mathrm{o}} \right) \boldsymbol{N} \, \mathrm{d}\Omega \tag{46}$$

$$\boldsymbol{C}_{\mathrm{og}} = \int_{\Omega_{\mathrm{e}}} \boldsymbol{W}^{\mathrm{T}} \left(n'_{\mathrm{l}} \rho_{\mathrm{o}} \right) \boldsymbol{N} \, \mathrm{d}\Omega \tag{47}$$

$$\boldsymbol{C}_{\mathrm{gw}} = \int_{\Omega_{\mathrm{e}}} \boldsymbol{W}^{\mathrm{T}} \left[\rho_{\mathrm{g}} \frac{n_{\mathrm{i}} C_{\mathrm{R}}}{n - n_{\mathrm{i}} C_{\mathrm{R}} (1 + p_{\mathrm{g}})} \left(n_{\mathrm{w}} + n'_{\mathrm{w}} p_{\mathrm{cow}} \right) \right] \boldsymbol{N} \, \mathrm{d}\Omega \tag{48}$$

$$\boldsymbol{C}_{\mathrm{go}} = \int_{\Omega_{\mathrm{e}}} \boldsymbol{W}^{\mathrm{T}} \left[n_{\mathrm{o}} \frac{R'_{\mathrm{so}} \rho_{\mathrm{gs}}}{B_{\mathrm{o}}} + \rho_{\mathrm{g}} \frac{n_{\mathrm{i}} C_{\mathrm{R}}}{n - n_{\mathrm{i}} C_{\mathrm{R}} (1 + p_{\mathrm{g}})} \left(n_{\mathrm{o}} - n'_{\mathrm{w}} p_{\mathrm{cow}} + n'_{\mathrm{l}} \left(\frac{n - n_{\mathrm{i}} C_{\mathrm{R}}}{n_{\mathrm{i}} C_{\mathrm{R}}} - p_{\mathrm{o}} \right) \right) \right] \boldsymbol{N} \, \mathrm{d}\Omega \tag{49}$$

$$\boldsymbol{f}_{\mathrm{w}} = \int_{\Omega_{\mathrm{e}}} \dot{M}_{\mathrm{w}} \boldsymbol{W}^{\mathrm{T}} \, \mathrm{d}\Omega - \int_{\Gamma_{\mathrm{q}}} \bar{q}_{\mathrm{w}} \boldsymbol{W}^{\mathrm{T}} \, \mathrm{d}\Gamma - \int_{\Gamma_{\mathrm{S.C.V.}}-\Gamma_{\mathrm{q}}} \left[\rho_{\mathrm{w}}^2 \left(\boldsymbol{K}_{\mathrm{w}} \boldsymbol{g} \right)^{\mathrm{T}} . \boldsymbol{n} \right] \boldsymbol{W}^{\mathrm{T}} \, \mathrm{d}\Gamma \tag{50}$$

$$\boldsymbol{f}_{\mathrm{o}} = \int_{\Omega_{\mathrm{e}}} \dot{M}_{\mathrm{o}} \boldsymbol{W}^{\mathrm{T}} \, \mathrm{d}\Omega - \int_{\Gamma_{\mathrm{q}}} \bar{q}_{\mathrm{o}} \boldsymbol{W}^{\mathrm{T}} \, \mathrm{d}\Gamma - \int_{\Gamma_{\mathrm{S.C.V.}}-\Gamma_{\mathrm{q}}} \left[\rho_{\mathrm{o}}^2 \left(\boldsymbol{K}_{\mathrm{o}} \boldsymbol{g} \right)^{\mathrm{T}} . \boldsymbol{n} \right] \boldsymbol{W}^{\mathrm{T}} \, \mathrm{d}\Gamma \tag{51}$$

$$\boldsymbol{f}_{\mathrm{g}} = \int_{\Omega_{\mathrm{e}}} \dot{M}_{\mathrm{g}} \boldsymbol{W}^{\mathrm{T}} \, \mathrm{d}\Omega - \int_{\Gamma_{\mathrm{q}}} \bar{q}_{\mathrm{g}} \boldsymbol{W}^{\mathrm{T}} \, \mathrm{d}\Gamma - \int_{\Gamma_{\mathrm{S.C.V.}}-\Gamma_{\mathrm{q}}} \left[\rho_{\mathrm{g}}^2 \left(\boldsymbol{K}_{\mathrm{g}} \boldsymbol{g} \right)^{\mathrm{T}} . \boldsymbol{n} \right] \boldsymbol{W}^{\mathrm{T}} \, \mathrm{d}\Gamma \tag{52}$$

where $\Omega_{\mathrm{S.C.V.}}$ and $\Gamma_{\mathrm{S.C.V.}}$ denote the domain of a sub-control volume and its faces, respectively; and $\boldsymbol{W}$ is the vector of the weighting functions. The weighting functions are chosen such that the ith weighting function of an element takes a constant value of unity over the sub-control volume belonging to node i, and zero elsewhere in the element, i.e.

$$W_i = \begin{cases} 1 & \text{in the sub-control volume belongs to node } i \\ 0 & \text{otherwise} \end{cases} \tag{53}$$

The temporal discretization of Eq. (38) is performed by the fully implicit first order accurate finite difference scheme

$$\begin{bmatrix} \boldsymbol{P}_{ww}+\Delta t\overline{\boldsymbol{P}}_{ww} & \boldsymbol{C}_{wo} & 0 \\ \boldsymbol{C}_{ow} & \boldsymbol{P}_{oo}+\Delta t\overline{\boldsymbol{P}}_{oo} & \boldsymbol{C}_{og} \\ \boldsymbol{C}_{gw} & \boldsymbol{C}_{go} & \boldsymbol{P}_{gg}+\Delta t\overline{\boldsymbol{P}}_{gg} \end{bmatrix}_{t+1} \begin{bmatrix} \Delta\hat{\boldsymbol{p}}_{w} \\ \Delta\hat{\boldsymbol{p}}_{o} \\ \Delta\hat{\boldsymbol{p}}_{g} \end{bmatrix}_{t+1} = \Delta t \begin{bmatrix} \boldsymbol{f}_{w} \\ \boldsymbol{f}_{o} \\ \boldsymbol{f}_{g} \end{bmatrix}_{t+1} - \Delta t \begin{bmatrix} \overline{\boldsymbol{P}}_{ww} & 0 & 0 \\ 0 & \overline{\boldsymbol{P}}_{oo} & 0 \\ 0 & 0 & \overline{\boldsymbol{P}}_{gg} \end{bmatrix}_{t+1} \begin{bmatrix} \hat{\boldsymbol{p}}_{w} \\ \hat{\boldsymbol{p}}_{o} \\ \hat{\boldsymbol{p}}_{g} \end{bmatrix}_{t} \tag{54}$$

where Δt is the time step length and $\Delta\hat{\boldsymbol{p}}_{n+1} = \hat{\boldsymbol{p}}_{n+1} - \hat{\boldsymbol{p}}_{n}$.

Eq. (54) represents a very large system of coupled and highly nonlinear equations on $(\Delta p_{\alpha})_{t+1}$ which should be solved by an appropriate iterative method. In the present work, the global inexact affine invariant Newton technique (GIANT) developed by Nowak and Weimann (1990) is employed to solve the system of Eq. (54). In this method, the global inexact Newton technique (Deuflhard, 1990) is combined with the fast secant method (Deuflhard et al, 1990), as an iterative linear solver, to obtain an efficient and robust numerical solution of a very large scale highly nonlinear system of equations. An algorithmic overview of the various parts of the calculations is given as a pseudo code in Table 2.

Table 2 Algorithmic outline of the various parts of calculations in the present model

```
Pre-processing and initializing
DO FOR EACH time step
    UPDATE variables and parameters
    DO FOR EACH Newton iteration
        DO FOR EACH element
            UPDATE the Jacobian matrix of Eq. (54)
            ASSEMBLE to the global Jacobian matrix
        END DO
        DOFOR EACH element
            UPDATE the residual of Eq. (54)
            ASSEMBLE of the global residual vector
        END DO
        DO
            Linear solver with fast secant method
            IF (Linear solver Conv. TRUE.) EXIT
        END DO
        IF (Newton Conv. TRUE.) THEN
          EXIT
        ELSE
          UPDATE variables
        END IF
    END DO
    Post-processing
END DO
END
```

4 Numerical experiments

The benchmark problems of the first and second comparative solution projects (CSP) of the SPE are used to evaluate the validity of the presented formulation and stability and convergence of the method to deal with a bubble-point and a three-phase coning problem. Furthermore, grid orientation effects on the results obtained by the model are investigated by a benchmark waterflooding example.

4.1 Gas displacement

This simulation problem is adopted from the first case of the benchmark problem of the first CSP (Odeh, 1981). This benchmark problem is a challenging case, and it was designed to evaluate the stability of black-oil reservoir simulators to deal with strong nonlinearity of the governing equations and transition of the reservoir condition from an undersaturated to a saturated state. The state of a reservoir is called undersaturated when it initially exists at a pressure higher than its bubble-point pressure. At the undersaturated condition, oil and water are the only fluid phases present in the reservoir. Whereas, at the saturated state of the reservoir, the free gas exists and its relatively high compressibility produces a strong source of nonlinearity in the governing equations. It is worth noting that the state of a location in a reservoir can change from saturated to undersaturated state, or vice versa, during the solution. The complete details of the problem can be found in Odeh (1981).

The results obtained by 7 organizations which participated in the solution project have been reported by Odeh (1981). A full description of the simulators used by these participants can be found in the reference. Generally, all the models were developed based on the traditional finite difference or finite volume methods. In this paper, the results obtained by the present model are compared with those obtained from two companies, namely, Shell Development Co. and Intercomp Resource Development and Engineering Inc..

Figs. 2 and 3 show the oil production rate and the gas-oil ratio obtained by the present model and those reported by Odeh (1981). As seen in the figure, the models show similar trends in the results, however a slight discrepancy is observed during 2.5 to 6.0 years. The maximum ratio of these differences is about 10% which is observed in the calculated oil production rates at 2.95 years.

The averaged pressure values in the blocks containing production and injection wells are compared with the results obtained by Shell Development Co. and Intercomp Resource

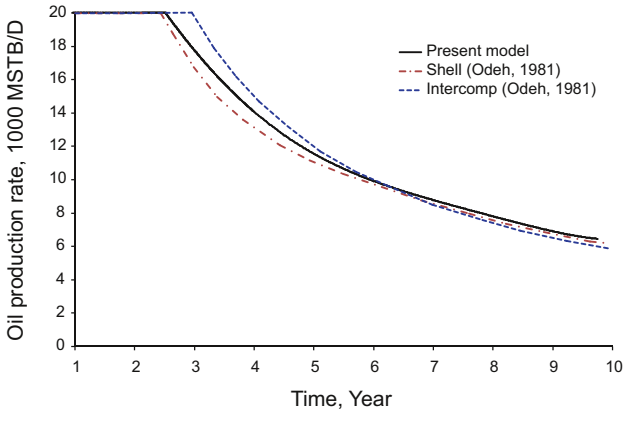

Fig. 2 Oil production rate versus time

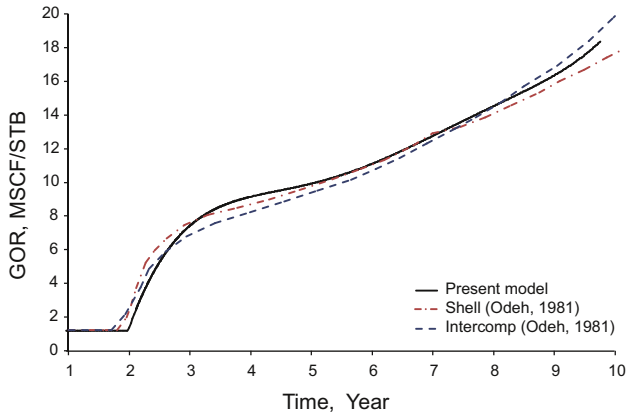

Fig. 3 Variation of the gas-oil ratio versus time

Development and Engineering Inc. in Figs. 4 and 5. Similar to Figs. 2 and 3 some slight discrepancies are also observed in these results. The maximum ratio of pressure discrepancy is about 8% which is occurred in the injection well block at 2 years. Fig. 6 shows the variation of gas saturation in the production block obtained by the present model and those reported by Odeh (1981).

A close study of our results reveals that the time of the increase of the GOR in Fig. 3 coincides with the time of the peak of reservoir pressure in the production block (Fig. 4), whereas the results obtained by the above mentioned companies show a small lag between these times. It is well known that the increase of GOR shows an increase in gas saturation in the production block and due to the lower viscosity of gas in compared with oil, the reservoir pressure at the production block will decrease. The coincidence of these two phenomena shows the superiority of our results in compared with the others.

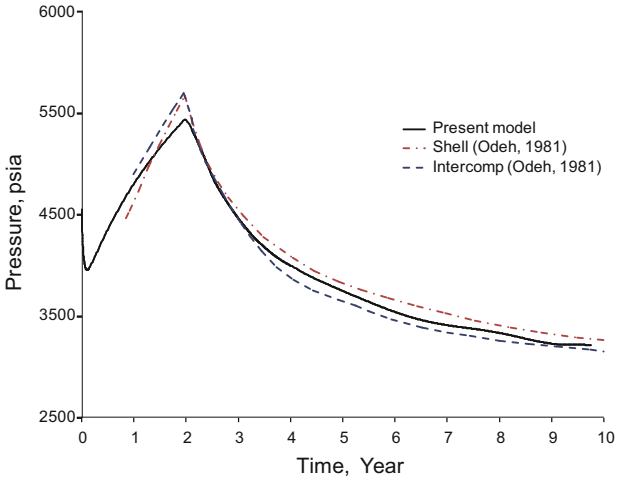

Fig. 4 Variation of pressure at the production well block versus time

4.2 Three-phase coning

The coning problem is the result of large gradient of a phase potential in the axis direction of a producing well (Fanchi, 2001). In the initial stage of the reservoir, the gradient of potential surface is zero everywhere. After a producer is perforated, the potential gradient would be created which tend to lower the gas-oil contact and elevate the water-

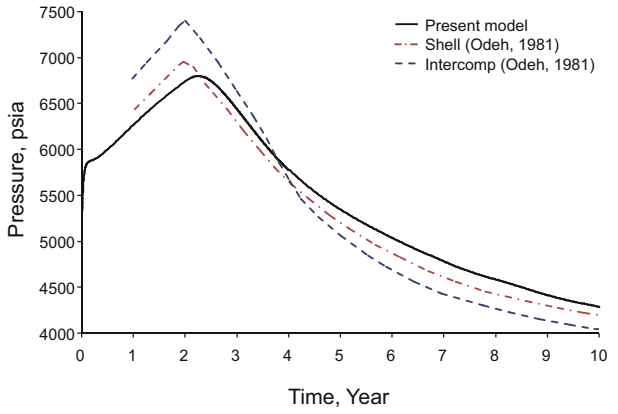

Fig. 5 Variation of pressure at the injection well block versus time

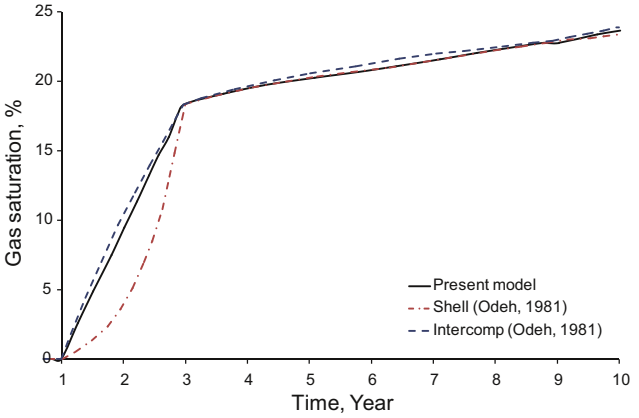

Fig. 6 Gas saturation at the production well block

oil contact around the production well. This potential gradient tends to deform the shape of the gas-oil and water-oil contacts into a cone. The top of the water cone and end of the gas cone gradually move toward the perforated zone of the producer. Therefore, the phase saturation and pressure will change very rapidly during the formation of the water and gas coning. This may cause instability in the numerical solution of the reservoir.

The second SPE CSP (Weinstein et al, 1986) is selected to evaluate the stability of the present numerical solution to deal with a coning problem. The required basic data of the problem are completely presented in Weinstein et al (1986).

Fig. 7 shows the plot of initial phase saturation versus depth. The gas saturation is equal to zero, below the depth

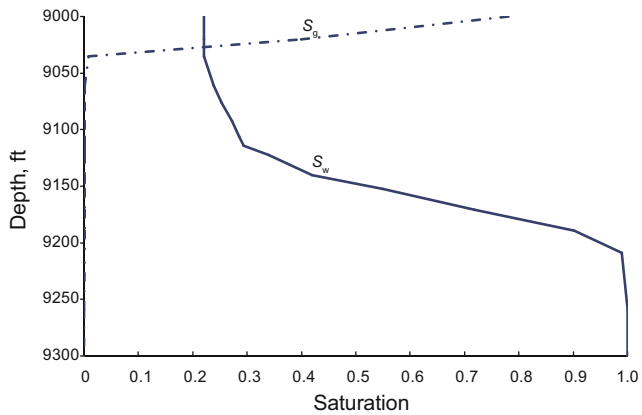

Fig. 7 Initial saturation distribution

of 9,035ft, and the water saturation is equal to 1 below the depth of 9,029 ft. These results are consistent with the given positions of the gas-oil contact and the oil-water contact. Also the initial saturations satisfy the constraint (15).

Figs. 8-10 present the plots of the oil production rate, water cut, and gas-oil ratio, respectively. These results are also compared with those obtained by two companies, namely, Shell Development Co. and Intercomp Resource Development and Engineering Inc. reported by Weinstein et al (1986). There are small differences (about 9%) between the results of the present model and those reported by Weinstein et al (1986).

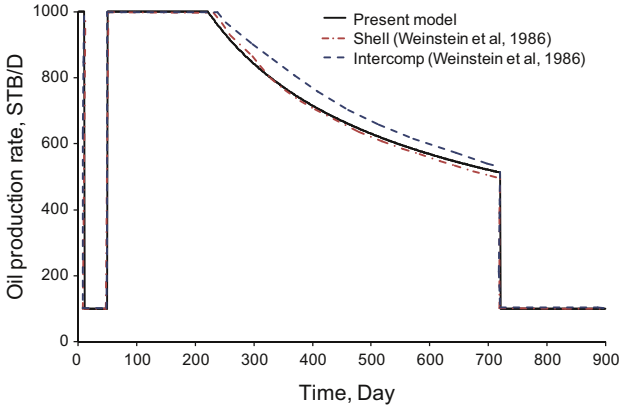

Fig. 8 Oil production rate versus time

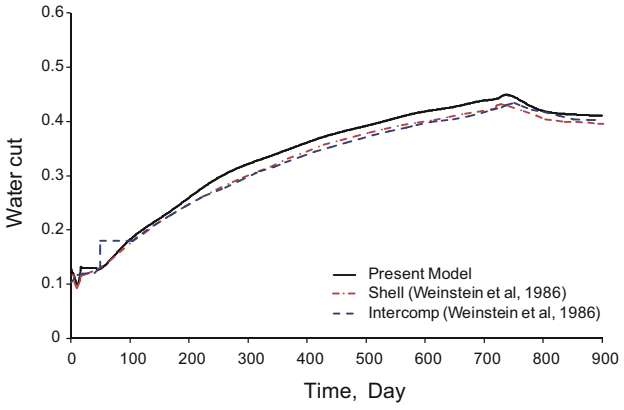

Fig. 9 Variation of water cut versus time

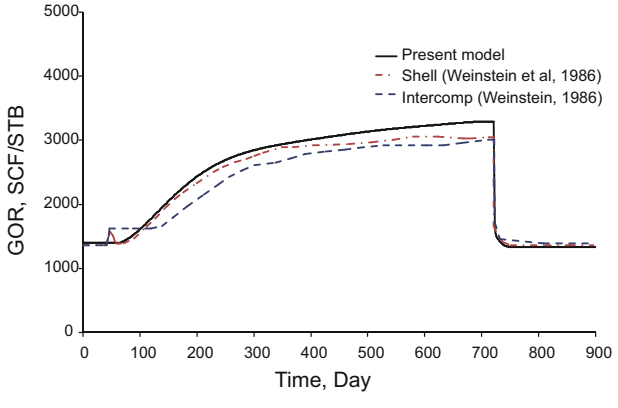

Fig. 10 Variation of gas-oil ratio versus time

4.3 Radial displacement

The problem analyzed in this section was proposed by Bajor and Cormack (1989) to evaluate the grid orientation effects. The geometry of this example, mesh generation of the domain and locations of the production and injection wells are illustrated in Fig. 11. The domain is initially saturated with 28% water and 72% oil. Initial zero pressure is assumed inside the domain. Water is injected to the domain with the rate of 0.8 m^3/day and the simulation is terminated after 2 PV (pore volume) of injection. The porosity and absolute permeability of the domain are considered 20.8% and 1500 mD, respectively. The viscosity of oil and water are considered 130 and 0.97 cP. The well radius and bottom-hole pressure for the production wells are considered to be 7.5 cm and zero, respectively. The capillary pressure and relative permeability functions are defined as below

$$p_c = 4.0 \times \left(\frac{n_w - 0.045}{0.1619} \right)^{-0.714} \tag{55}$$

$$\begin{cases} k_{rw} = \left(\dfrac{n_w - 0.045}{0.1619} \right)^{4.429} \\ k_{ro} = \left(1 - \dfrac{n_w - 0.045}{0.1619} \right)^2 \left[1 - \left(\dfrac{n_w - 0.045}{0.1619} \right)^{2.429} \right] \end{cases} \tag{56}$$

It is worth noting that the oil and water, in this example, are considered as two immiscible and incompressible fluids.

Regarding the geometry of the domain, water production should be identical at all of the producers. Therefore, diversity of water cut curves for different producers can reflect the effect of grid orientation. Fig. 12 depicts the maximum difference of the water cut curves among the producers. The maximum value of discrepancy between the producers is about 2.5 percent.

To check the effect of grid distribution on the results of the model, the number of grids is increased from 192 elements to 307 elements. Figs. 13 and 14 compare the water saturation contours and variation of pressure at the injection block, respectively. As seen in the figures, the solution with 307

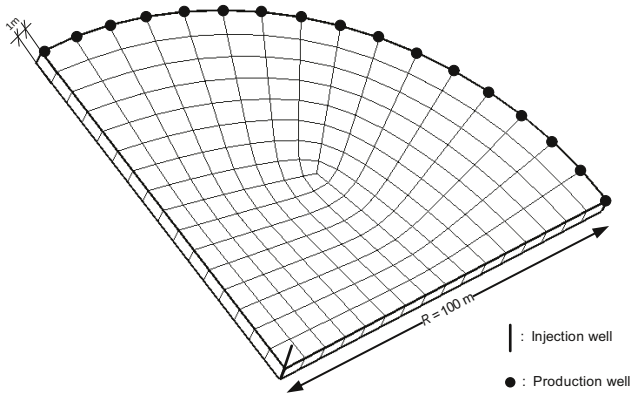

Fig. 11 Geometric configuration of example 3

elements is in good agreement with the former. Regarding to these results, one could conclude that sensitivity of the method to the grid orientation is very low. These figures also demonstrate the convergence of numerical solution scheme.

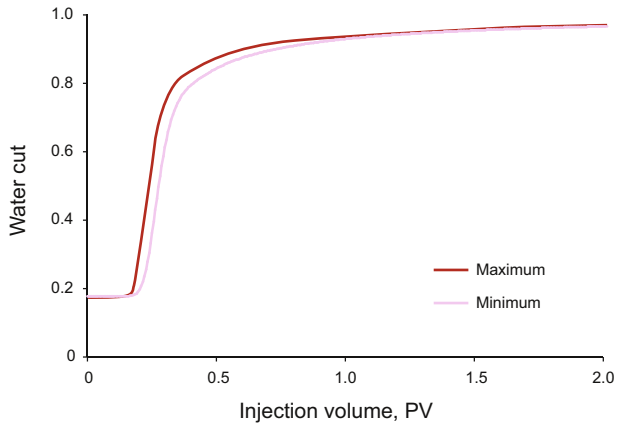

Fig. 12 Maximum and minimum of water cut at the production wells

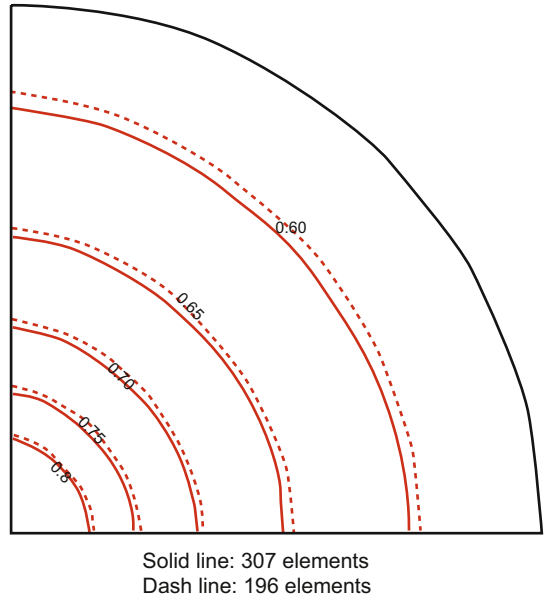

Fig. 13 Water saturation contour after 2 PV of water injection

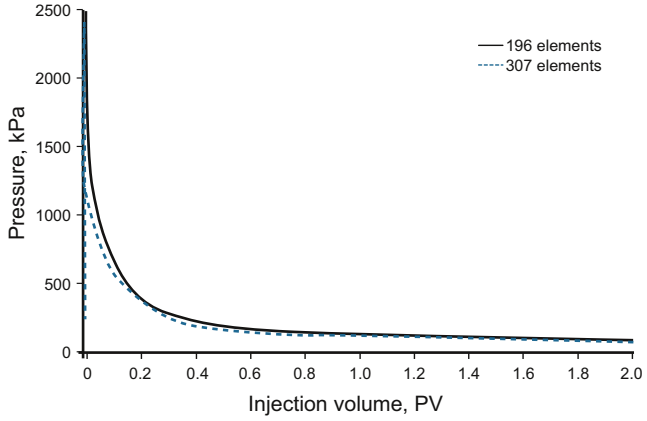

Fig. 14 Variation of pressure at the injection block

Fig. 15 shows the distribution of local mass balance error for the present test case. As it is seen in the figure, for the injection rate of 0.8 m^3/day, the local mass balance error is in the range of 10^{-7} m^3/day. Fig. 16 describes the cumulative global mass balance error over injection time. Dividing the error by the total flow rate of 0.8 m^3/day, we get less than 10^{-4}% errors. These figures show that the present model is a fully conservative scheme.

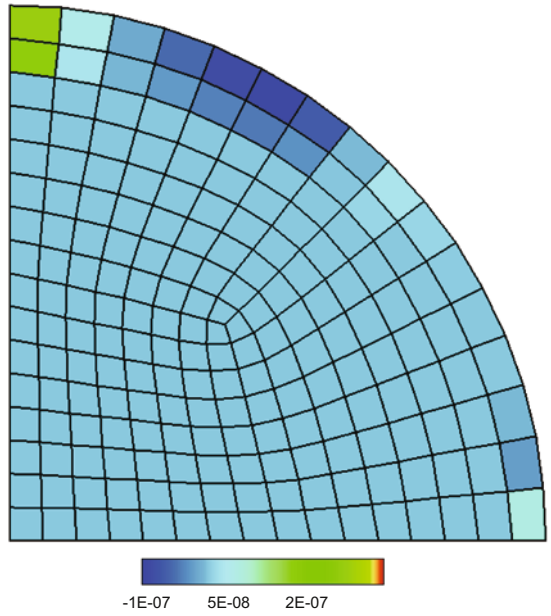

Fig. 15 Distribution of local mass balance error

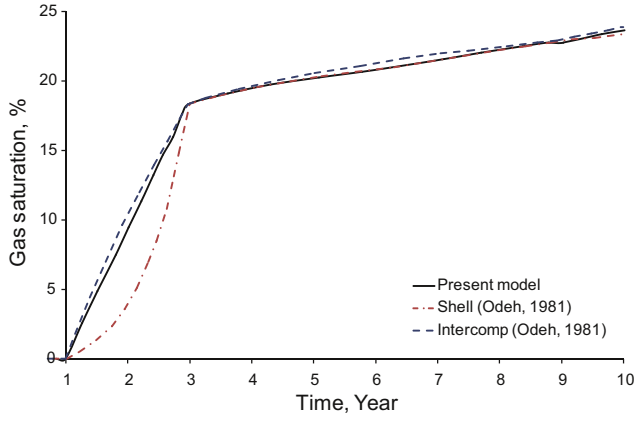

Fig. 16 Cumulative global mass balance error over injection time

5 Conclusions

In this paper, a fully coupled control volume finite element model is developed to simulate the black-oil flow in hydrocarbon reservoirs. The method is fully conservative and able to deal with unstructured grid systems. It combines the mesh flexibility of FEM with the local conservative characteristic of FDM and consequently overcomes the deficiencies of FDM in dealing with geometrically complex reservoirs, or inability of FEM to conserve mass locally. Local and global conservative characteristic of the method

is evaluated with a representative example. The numerical experiments show that the method is accurate, stable and convergent even in dealing with bubble-point and coning problems which are the well-known difficult and unstable problems in the field of reservoir simulation. Furthermore, effects of mesh orientation on the results obtained by the present formulation are investigated. Based on the numerical results, grid sensitivity of the formulation is very low and could be neglected. Currently, we are investigating the possible extension of this methodology to deal with the solution of the coupled geomechanic and multiphase flow equations.

Acknowledgements

The authors would like to thank Iranian Offshore Oil Company (IOOC) for financial support of this work.

References

Aavatsmark I. An introduction to multipoint flux approximations for quadrilateral grids. Comput. Geosci. 2002. 6: 405-432

Aronofsky J and Jenkins R. A simplified analysis of unsteady radial gas flow. Transactions of AIME. 1954. 201: 149-154

Bajor O and Cormack D. A new method for characterizing the grid orientation phenomenon. Society of Petroleum Engineering. 1989 (paper SPE 19353)

Bergamaschi L, Mantica S and Manzini G. A mixed finite element-finite volume formulation of the black-oil model. SIAM J. Sci. Comput. 1998. 20: 970-997

Brand W, Heinemann J and Aziz K. The grid orientation effect in reservoir simulation. Symposium on Reservoir Simulation. 1991. (paper SPE 21228)

Cancelliere and Verga. Simulation of unconventional well tests with the finite volume method. Petrol. Sci. 2012. 9(3): 317-329

Carvalho D, Willmersdorf R and Lyra P. A node-centered finite volume formulation for the solution of two-phase flows in non-homogeneous porous media. Int. J. Numer. Meth. Fluids. 2007. 53: 1197-1219

Chen Z, Huan G and Wang H. Computer simulation of compositional flow using unstructured control volume finite element methods. Computing. 2006. 78: 31-53

Coats K, Thomas K and Pierson R. Compositional and black oil reservoir simulation. SPE Reservoir Evaluat. Eng. 1998. 1: 372-379

Cordazzo J, Maliska C and Romeu R. Considerations about the internodal permeability evaluation in reservoir simulation. The 2nd Brazilian Congress on R&D in Petroleum and Gas, June 2003, Rio de Janeiro

Cordazzo J, Maliska C, Silva A, et al. The negative transmissibility issue when using CVFEM in petroleum reservoir simulation—1. Theory. Proceedings of the 10th Brazilian Congress of Thermal Sciences and Engineering -ENCIT 2004, Braz. Soc. of Mechanical Sciences and Engineering -ABCM, Nov. 2004a, Rio de Janeiro

Cordazzo J, Maliska C, Silva A, et al. The negative transmissibility issue when using CVFEM in petroleum reservoir simulation—2. Results. Proceedings of the 10th Brazilian Congress of Thermal Sciences and Engineering -ENCIT 2004, Braz. Soc. of Mechanical Sciences and Engineering -ABCM, Nov. 2004b, Rio de Janeiro

Deuflhard P. Global inexact Newton methods for very large scale nonlinear problems. Konrra-Zuse-Zentrum fuer Informationstechnik Berlin. 1990

Deuflhard P. Freund R and Walter A. Fast secant methods for the iterative solution of large nonsymmetric linear systems. IMPACT Comput. Sci. Eng. 1990. 2: 244-276

Durlofsky L. A triangle based mixed finite element-finite volume technique for modeling two phase flow through porous media. J. Comput. Phys. 1993. 105: 252-266

Durlofsky L and Aziz K. Advanced techniques for reservoir simulation and modeling of nonconventional wells. Final Report, Stanford University. 2004

Durlofsky L, Engquist B and Osher S. Triangle based adaptive stencils for the solution of hyperbolic conservation laws. J. Comput. Phys. 1992. 98: 64-75

Edwards M. Unstructured control-volume distributed full tensor finite-volume schemes with flow based grids. Computa. Geosci. 2002. 6: 433-445

Edwards M and Rogers C. Finite volume discretization with imposed flux continuity for the general tensor pressure equation. Comput. Geosci. 1998. 2: 259-290

Eikemo B, Lie K, Eigestad G T, et al. Discontinuous Galerkin methods for advective transport in single-continuum models of fractured media. Adv. Water Resour. 2009. 32(4): 493-506

Ewing R. The Mathematics of Reservoir Simulation. SIAM. 1983

Fanchi J. Principles of Applied Reservoir Simulation (2nd Ed.). Gulf Professional Publishing. 2001

Fanchi J R, Harpole K J and Bujnowski S W. BOAST: A three-dimensional, three-phase black oil applied simulation tool (version 1.1). United States Department of Energy. 1982

Flemisch B, Darcis M, Erbertseder K, et al. DuMu^x: DUNE for multi-{phase, component, scale, physics, …} flow and transport in porous media. Adv. Water Resour. 2011. 34: 1102-1112

Forsyth P. A control-volume, finite-element method for local mesh refinement. SPE Reservoir Engineering. 1990. 5(4): 561-566 (paper SPE 18415)

Fung L, Hiebert A and Nghiem L. Reservoir simulation with a control volume finite element method. SPE Reservoir Engineering. 1992. 7(3): 349-357 (paper SPE 21224)

Geiger S, Roberts S, Matthai S, et al. Combining finite element and finite volume methods for efficient multiphase flow simulations in highly heterogeneous and structurally complex geologic media. Geofluids. 2004. 4: 284-299

Goodman M and Gowin S C. A continuum theory for granular materials. Arch. Rat. Mech. Anal. 1972. 44: 249-266

Gottardi G and Dall´Olio D. A control-volume finite-element model for simulating oil-water reservoirs. J. Petrol. Sci. Eng. 1992. 8: 29-41

Hassanizadeh M and Gray W G. Thermodynamic basic of capillary pressure in porous media. Water Resour. Res. 1993. 29: 3389-3405

Hoteit H and Firoozabadi A. Numerical modeling of two-phase flow in heterogeneous permeable media with different capillarity pressures. Adv. Water Resour. 2008. 31: 56-73

Katyal A K, Kaluarachchi J J, and Parker J C. MOFAT: A two-dimensional finite element program for multiphase flow and multicomponent transport, program documentation and user's guide. Center for Environmental and Hazardous Materials Studies Virginia Polytechnic Institute and State University. 1991

Lee S, Wolfsteiner C and Tchelepi H. Multiscale finite-volume formulation for multiphase flow in porous media: black oil formulation of compressible, three-phase flow with gravity. Comput. Geosci. 2008. 12: 351-366

Li B, Chen Z and Huan G. The sequential method for the black-oil reservoir simulation on unstructured grids. J. Comput. Phys. 2003. 192: 36-72

Li B, Chen Z and Huan G. Control volume function approximation methods and their applications to modeling porous media flow II: the black oil model. Adv. Water Resour. 2004. 27: 99-120

Li W, Chen Z, Ewing R, et al. Comparison of the GMRES and ORTHOMIN for the black oil model in porous media. Int. J. Numer. Meth. Fluids. 2005. 48: 501-519

Lu Q, Malgorzata P and Gai X. Implicit black-oil model in IPARS framework IPARSv2, Model I, keyword BLACKI, Version 1.1. Texas Institute for Computational and Applied Mathematics, The University of Texas at Austin. 2001

Matthäi S K, Geiger S, Roberts S G, et al. Numerical simulation of multi-phase fluid flow in structurally complex reservoirs. Geological Society, London, Special Publications. 2007. 292: 405-429

Monteagudo J and Firoozabadi A. Control-volume model for simulation of water injection in fractured media: incorporating matrix heterogeneity and reservoir wettability effects. SPE J. 2007. 12: 355-366

Naderan H, Manzari M T and Hannani S K. Application and performance comparison of high-resolution central schemes for black oil model. Int. J. Num. Meth. for Heat & Fluid Flow. 2007. 17(7): 736-753

Nick H M and Matthäi S K. Comparison of three FE-FV numerical schemes for single- and two-phase flow simulation of fractured porous media. Transp. Porous Med. 2011. 90: 421-444

Nowak U and Weimann L. GIANT: A software package for the numerical solution of very large systems of highly nonlinear equations. Konrra-Zuse-Zentrum fuer Informationstechnik Berlin. 1990

Odeh A. Comparison of solutions to a three-dimensional black-oil reservoir problem. J. Pet. Tech. 1981. 13-25

Pao W K, Lewis R W and Masters I. A fully coupled hydro-thermo-mechanical model for black oil reservoir simulation. Int. J. Numer. Anal. Meth. Geomech. 2001. 25: 1229-1256

Pruess K, Oldenburg C and Moridis G. TOUGH2 user's guide, version 2. Earth Science Division, Lawrence Berkeley National Laboratory. 2012

Reichenberger V, Jakobs H, Bastian P, et al. A mixed-dimensional finite volume method for two-phase flow in fractured porous media. Adv. Water Resour. 2006. 29: 1020-1036

Romeu R and Noetinger B. Calculation of internodal transmissibilities in finite difference models of flow in heterogeneous porous media. Water Resour. Res. 1995. 31(4): 943-959

Sadrnejad S A, Ghasemzadeh H, Ghoreishian Amiri S A, et al. A control volume based finite element method for simulating incompressible two-phase flow in heterogeneous porous media and its application to reservoir engineering. Petrol. Sci. 2012. 9(4): 485-495

Settari A and Aziz K. Treatment of nonlinear terms in the numerical solution of partial differential equations for multiphase flow in porous media. Int. J. Multiphase Flow. 1975. 1: 817-844

Simbnek J, Huang K, and Van Genuchten M Th. The SWMS- 3D code for simulating water flow and solute transport in three-dimensional variably-saturated media. U.S. Salinity Laboratory, Agricultural Research Service, U.S. Department of Agriculture, Riverside, California. 1995

Verma S. Flexible grids for reservoir simulation. Ph.D. Thesis. Department of Petroleum Engineering, University of Stanford. 1996

Wan J. Stabilized finite element methods for coupled geomechanics and multiphase flow. Ph.D. Thesis. Stanford University. 2002

Wang W, Rutqvist J, Görke U J, et al. Non-isothermal flow in low permeable porous media: a comparison of Richards' and two-phase flow approaches. Environ. Earth. Sci. 2011. (62): 1197-1207

Weinstein H, Chappelear J and Nolen J. Second comparative solution project: A three-phase coning study. J. Pet. Tech. 1986. 345-353

White M D and Oostrom M. STOMP: Subsurface Transport Over Multiple Phases, version 2, theory guide. U.S. Department of Energy, 2000

Young L. An efficient finite element method for reservoir simulation. Proceedings of the 53rd SPE Annual Technical Conference and Exhibition, Houston, 1978 (paper SPE 7413)

(Edited by Sun Yanhua)